

To be published in the Astrophysical Journal

## Revealing $\delta$ Cephei's Secret Companion and Intriguing Past

R.I. Anderson<sup>1,2,4</sup>, J. Sahlmann<sup>3</sup>, B. Holl<sup>2</sup>, L. Eyer<sup>2</sup>, L. Palaversa<sup>2</sup>, N. Mowlavi<sup>2</sup>, M. S  veges<sup>2</sup>, M. Roelens<sup>2</sup>

<sup>1</sup>*Department of Physics and Astronomy, Johns Hopkins University, Baltimore, MD 21218, USA*

<sup>2</sup>*D  partement d'Astronomie, Universit   de Gen  ve, 51 Ch. des Maillettes, 1290 Sauverny, Switzerland*

<sup>3</sup>*European Space Agency, European Space Astronomy Centre, P.O. Box 78, Villanueva de la Ca  nada, 28691 Madrid, Spain*

ria@jhu.edu

### ABSTRACT

Classical Cepheid variable stars are crucial calibrators of the cosmic distance scale thanks to a relation between their pulsation periods and luminosities. Their archetype,  $\delta$  Cephei, is an important calibrator for this relation. In this paper, we show that  $\delta$  Cephei is a spectroscopic binary based on newly-obtained high-precision radial velocities. We combine these new data with literature data to determine the orbit, which has period 2201 days, semi-amplitude  $1.5 \text{ km s}^{-1}$ , and high eccentricity ( $e = 0.647$ ). We re-analyze *Hipparcos* intermediate astrometric data to measure  $\delta$  Cephei's parallax ( $\varpi = 4.09 \pm 0.16 \text{ mas}$ ) and find tentative evidence for an orbital signature, although we cannot claim detection. We estimate that *Gaia* will fully determine the astrometric orbit. Using the available information from spectroscopy, velocimetry, astrometry, and Geneva stellar evolution models ( $M_{\delta\text{Cep}} \sim 5.0 - 5.25 M_{\odot}$ ), we constrain the companion mass to within  $0.2 < M_2 < 1.2 M_{\odot}$ . We discuss the potential of ongoing and previous interactions between the companion and  $\delta$  Cephei near pericenter passage, informing reported observations of circumstellar material and bow-shock. The orbit may have undergone significant changes due to a Kozai-Lidov mechanism

---

<sup>4</sup>Swiss National Science Foundation Fellow

driven by the outer (visual and astrometric) companion HD 213307. Our discovery of  $\delta$  Cephei’s nature as a spectroscopic binary exposes a hidden companion and reveals a rich and dynamical history of the archetype of classical Cepheid variables.

*Subject headings:* binaries: general, binaries: spectroscopic, stars: distances, stars: individual:  $\delta$  Cephei = HD 213306 = HIP 110991, stars: oscillations, stars: variables: Cepheids

## 1. Introduction

Classical Cepheid variable stars (from hereon: Cepheids) are precise Galactic and extragalactic distance tracers and thus of crucial importance for cosmology. The prototype of this class of stars,  $\delta$  Cephei (HD 213306, HIP 110991), has been extensively<sup>1</sup> studied ever since the discovery of its variability 230 years ago by Goodricke (1786). Until Baade’s proposed method (Baade 1926) to test Shapley’s pulsation hypothesis (Shapley 1914) bore fruit in the early to mid 20th century, Cepheids were thought to be binary stars on eccentric orbits (see e.g. Gautschy 1997), inspiring a great deal of research, not least that by Christian Doppler.

The first scientists to measure the variability of  $\delta$  Cephei’s spectral lines and to determine their velocities were Belopolsky (1894, 1895) and Moore (1913), before radial velocities (RVs) became available for many Cepheids thanks to the observations by Joy (1937). Two decades later, Shane (1958) conducted a detailed analysis of  $\delta$  Cephei’s RV curve and concluded that no evidence of long-period changes in the mean velocity could be seen, a result that was confirmed much later by Kovacs et al. (1990).

Nowadays, Cepheids are known to be pulsating variable stars, although many Cepheids are also known to be binaries<sup>2</sup>. The binary fraction of Cepheids is being studied intensively with most recent estimates of the total binary fraction ranging around 60%, see e.g. Evans et al. (2013) and Szabados et al. (2013). However, Cepheids cannot reside in very close-in binary systems (e.g. Neilson et al. 2014) due to their nature as evolved (super-)giant stars, which results in observed minimum orbital periods of approximately one year. For long periods ( $> 10$  years), practical constraints create significant observational bias against companion detection.

---

<sup>1</sup>SIMBAD (<http://simbad.u-strasbg.fr>) lists more than 600 articles related to  $\delta$  Cephei.

<sup>2</sup>cf. the Cepheid binary database by Szabados (2003) at <http://www.konkoly.hu/CEP/nagytab3.html>

To our knowledge,  $\delta$  Cephei has not been shown to be a spectroscopic binary prior to this work.  $\delta$  Cephei is, however, a known *visual* binary (Ferne 1966), whose companion HD 213307 (= HIP 110988) is itself an astrometric binary and thought to be physically associated (see Benedict et al. 2002, and references therein). HD 213307 was proposed to also be a spectroscopic binary (Herbig, priv. comm. mentioned in Ferne 1966). Finally,  $\delta$  Cephei is usually considered to be a member of the loose association Cepheus OB6 (de Zeeuw et al. 1999; van Leeuwen et al. 2007; Majaess et al. 2012).

Precise trigonometric parallax of  $\delta$  Cephei has been measured by Perryman & ESA (1997), van Leeuwen et al. (2007), and van Leeuwen et al. (2007) using observations made by the *Hipparcos* space mission and by Benedict et al. (2002) using measurements obtained with FGS 3 on board the Hubble space telescope (*HST*). Notable previous distance estimates include those reported by Fernley et al. (1989), Gieren et al. (1993), Gatewood et al. (1993), Mourard et al. (1997).

Mérand et al. (2005) employed infrared long-baseline interferometry to study the Baade-Wesselink projection factor of  $\delta$  Cephei and were later (Mérand et al. 2006) able to show the presence of an extended circumstellar envelope. The presence of this circumstellar environment was confirmed independently (using different methodologies) by Marengo et al. (2010) and Matthews et al. (2012).

In this paper, we present the discovery of the spectroscopic binary nature of  $\delta$  Cephei. This discovery is demonstrated using new observations that are presented in Sect. 2. Using these new data we reveal the presence of a hidden companion in Sect. 3.1. After combining our new RVs with literature data in Sect. 3.2, we determine the orbital solution in Sect. 3.3. We re-analyze the *Hipparcos* intermediate astrometric data from the van Leeuwen (2007) reduction in Sects. 4.1.1 and 4.1.2 to measure parallax and to investigate whether the available astrometric measurements are sensitive to the motion due to binarity. In Sect. 4.2, we investigate *Gaia*’s expected sensitivity to the binary motion. We discuss how our discovery helps to better interpret other observations and begins to draw a complex picture of  $\delta$  Cephei’s rich and dynamical history in Sect. 5 before concluding in Sect. 6.

## 2. New *Hermes* Observations

Line-of-sight (radial) velocities were measured from 136 observations taken between September 2011 and September 2014 using the fiber-fed high-resolution ( $R \sim 85\,000$ ) spectrograph *Hermes* (Raskin et al. 2011) at the Flemish 1.2m Mercator telescope located at Roque de los Muchachos Observatory, La Palma, Canary Islands. We utilize the high-

resolution fiber (HRF) mode for all observations, since this is the most commonly used, i.e., best-understood, observing mode available for *Hermes*. The HRF mode offers optimal efficiency and the highest available spectral resolution.

The reduction pipeline available for *Hermes* performs pre- and overscan bias correction, flatfielding using Halogen lamps, and background modelization, as well as cosmic ray removal. ThAr lamps are used for the wavelength calibration. RVs are determined via the cross-correlation technique (Baranne et al. 1996; Pepe et al. 2002) using a numerical mask designed for solar-like stars (optimized for spectral type G2).

These observations were started as part of a search for Cepheids belonging to open clusters (Anderson et al. 2013) with the goal of quantifying the precision limit for a classical Cepheid using *Hermes* RVs and of having high-quality spectra available for further study. The average signal-to-noise ratio of the spectra is higher than 200 near 6000 Å, with some spectra reaching up to 400.

Table 1 shows a sample of our *Hermes* RV measurements that we are making publicly available at the CDS<sup>3</sup> together with our standard star observations.

## 2.1. Zero-point, Stability, and Precision of *Hermes* RVs

To determine the RV zero-point of *Hermes*, we observed eight RV standard stars listed in Udry et al. (1999a,b)<sup>4</sup>, see Tab. 2. These standard stars were chosen to cover the range of spectral types that  $\delta$  Cephei exhibits during its pulsation cycles. We thus determine a mean systematic offset of  $55 \text{ m s}^{-1}$  with respect to the *ELODIE* and *CORAVEL* zero-point. We estimate this zero-point offset to be accurate to approximately  $10 \text{ m s}^{-1}$  and note that additional scatter in the difference between *Hermes* and literature RVs can exist for various reasons of astrophysical origin, including binarity and planetary companions. We therefore increase our error margin by adding  $10 \text{ m s}^{-1}$  in quadrature to the *Hermes* RV uncertainties when correcting for zero-point offsets.

We investigate the long-term stability and precision of *Hermes* RVs using the RV standard star observations. Thanks to the very high signal-to-noise ratio of our spectra, photon-noise (Bouchy et al. 2001) contributes only marginally to the uncertainty of our *Hermes* RVs. Instead, the precision of our RVs is dominated by the intra-night stability of the wavelength

---

<sup>3</sup><http://cds.u-strasbg.fr/>

<sup>4</sup>see [http://obswww.unige.ch/\\$\sim\\$udry/std/std.html](http://obswww.unige.ch/$\sim$udry/std/std.html)

| BJD - 2 400 000             | Phase   | $v_r$<br>[ km s <sup>-1</sup> ] | $\sigma(v_r)$<br>[ km s <sup>-1</sup> ] |
|-----------------------------|---------|---------------------------------|---|
| 55816.469627                | 0.82074 | 0.802                           | 0.018                                   |
| 55816.470920                | 0.82098 | 0.813                           | 0.018                                   |
| 55816.472221                | 0.82122 | 0.824                           | 0.018                                   |
| 55817.510667                | 0.01474 | -21.125                         | 0.018                                   |
| 55817.511961                | 0.01498 | -21.202                         | 0.018                                   |
| 55818.494094                | 0.19800 | -31.354                         | 0.018                                   |
| 55818.495384                | 0.19824 | -31.362                         | 0.018                                   |
| 55818.496675                | 0.19848 | -31.342                         | 0.018                                   |
| 55819.497269                | 0.38494 | -21.989                         | 0.018                                   |
| 55819.498564                | 0.38518 | -21.984                         | 0.018                                   |
| full table available at CDS |         |                                 |   |

Table 1: Sample of the new *Hermes* RV data that are published in their entirety at the CDS, and shown here for guidance regarding their form and content. Radial velocities have been shifted to the *CORAVEL-ELODIE* zero-point. Pulsation phase is defined here as 0 when  $v_r = v_\gamma$  at the steep part of the RV curve. Uncertainties are fixed at 18 m s<sup>-1</sup> to account for uncertainty in the wavelength calibration and zero-point calibration, see text.

| HD     | Sp.Type | $\langle v_r \rangle$<br>[km s <sup>-1</sup> ] | $v_{r,\text{ref}}$<br>[km s <sup>-1</sup> ] | $\Delta v_{r,\text{ref}}$<br>[km s <sup>-1</sup> ] | RMS <sub>nc</sub><br>[m s <sup>-1</sup> ] | RMS <sub>corr</sub><br>[m s <sup>-1</sup> ] |
|--------|---------|--|---|--|---|---|
| 10780  | K0V     | 2.771  | 2.70  | 0.071  | 38.7                                      | 17.1  |
| 32923  | G4V     | 20.627   | 20.50                                       | 0.127  | 70.1                                      | 14.8  |
| 42807  | G2V     | 6.068  | 6.00  | 0.068  | 115.2                                     | 29.7  |
| 82106  | K3V     | 29.784   | 29.75                                       | 0.034  | 45.8                                      | 20.8  |
| 144579 | G8V     | -59.452  | -59.45                                      | -0.002   | 42.7                                      | 20.0  |
| 168009 | G1V     | -64.581  | -64.65                                      | 0.069  | 36.4                                      | 20.0  |
| 197076 | G5V     | -35.413  | -35.40                                      | -0.013   | 78.3                                      | 10.9  |
| 221354 | K0V     | -25.111  | -25.20                                      | 0.089  | 53.8                                      | 15.5  |

Table 2: List of RV standard stars with spectral types from SIMBAD, *Hermes* RVs of standard stars from new observations, Udry et al. (1999b), offsets between new and reference RVs, and RMS of new observations without (subscript nc) and with pressure corrections applied (subscript corr) following Anderson (2013, Sec. 2.1.5).

calibration and the long-term stability of the instrument.

To improve RV precision and stability, we employ a method developed in Anderson (2013, Sec. 2.1.5) to correct for the RV drift induced by atmospheric pressure variations that occur during the night. Pressure variations are the leading cause for drifts in *Hermes* RVs, since the temperature of the instrument is stabilized to within  $0.01^\circ\text{K}$  (Raskin et al. 2011). The RV drift correction due to pressure variations is based on changes in the refractive index of air and has been shown to be precise to approximately  $10\text{ m s}^{-1}$  in the case of the *Coralie* spectrograph<sup>5</sup> for which RV drift corrections are measured using interlaced simultaneous ThAr exposures. For *Hermes*, our method improves RV precision by a factor of approximately 2.5, as measured by the decrease in RMS for all standard stars.

Figure 1 shows both the uncorrected (red dashed lines) and corrected RVs (blue solid line) for the standards stars HD 144579 and HD 168009 as a function of time for the different observing runs during which they were observed. The highest precision of  $9\text{ m s}^{-1}$  is achieved for HD 168009 during a ten-night observing run in July 2013. We find no evidence for long-term variations over the 3 year duration of the observations. Based on all standard star measurements, we estimate the long-term precision of pressure-corrected *Hermes* RVs to be approximately  $15\text{ m s}^{-1}$ . Accounting for the additional uncertainty due to zero-point offsets (see above), we adopt  $18\text{ m s}^{-1}$  as our error budget for the investigations based purely on *Hermes* RVs<sup>6</sup>. Note that this adopted uncertainty of  $18\text{ m s}^{-1}$  is more than a factor 2000 smaller than the pulsation-induced peak-to-peak RV amplitude of  $38.6\text{ km s}^{-1}$ .

### 3. Results from Spectroscopy

In this section we describe our analysis of  $\delta$  Cephei’s RV curve, starting with the initial discovery of  $\delta$  Cephei’s nature as a spectroscopic binary (Sect. 3.1). After subtracting the RV drift due to orbital motion observed in *Hermes* data, we establish a high-precision reference model for the pulsations alone, which we subtract from a combined data set of RVs from *Hermes* and several literature sources (cf. Sect. 3.2). Using this combined dataset, we determine the orbit for the binary system in Sect. 3.3.

We also searched the individual high-quality *Hermes* spectra as well as the cross-correlation profiles for a signature identifying the companion, finding none. We note that previous analyses of IUE (Evans et al. 1993) and HST/COS (Engle et al. 2014) spectra did

---

<sup>5</sup>*Coralie* is mounted to the Swiss 1.2m Euler telescope located at La Silla Observatory, Chile

<sup>6</sup>However, the uncertainty adopted to determine  $\delta$  Cephei’s orbit is  $47\text{ m s}^{-1}$ , cf. Sect. 3.1 and Fig. 4.

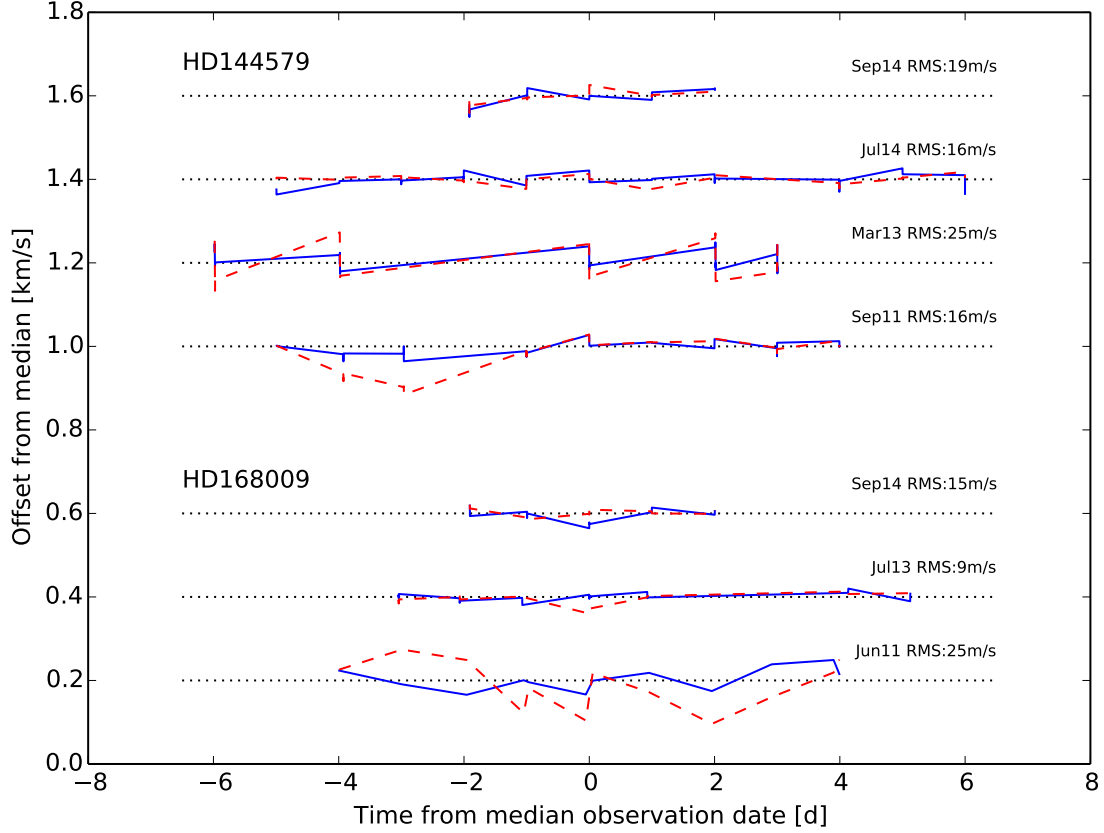


Fig. 1.— Hermes RV standard stars HD 144579 and HD 168009. The measurements are separated into individual observing runs and plotted as a function of time centered around the median observation date of a given star in a given observing run. We plot the measurements as residuals around the median of all measurements (i.e., including data from all observing runs) as listed in Tab. 2. We offset measurements from different observing runs and different stars (black dotted line) from one another for clarity. Pressure-corrected (see text) measurements are shown as solid blue connected dots, the uncorrected measurements are shown as a red dashed line. The labels on the right indicate observing run and RMS of the pressure-corrected RVs.

not report evidence of a companion’s signature, effectively ruling out early-type companions. Given the high signal-to-noise ratio (S/N) of our spectra and the even better S/N of the cross-correlation profiles, we estimate that the companion must be at least a factor 100 fainter than  $\delta$  Cephei, at least in optical bandpasses. Based on Geneva stellar evolution models (Georgy et al. 2013) and assuming an approximately  $5 M_{\odot}$  Cepheid, this implies a companion mass below approximately  $1.75 M_{\odot}$ . This is consistent with the upper limit on companion spectral type (A3, i.e.,  $M_2 < 2 M_{\odot}$ ) set by non-detection in IUE spectra (Evans 1992).

### 3.1. Discovery of $\delta$ Cephei B using HERMES RVs

Figure 2 shows the *Hermes* RVs obtained for  $\delta$  Cephei, phase-folded with the best-fitting pulsation period of  $P_{\text{puls}} = 5.366274$  d. The ten-fold RV uncertainty is shown in the upper right corner. The observation date is traced by symbol color going from red (first observations in September 2011) to yellow (September 2014). The color coding reveals the average radial velocity to be time-dependent, thus revealing orbital motion caused by a hidden companion.

We model the RV variations due to pulsation using the technique described in Anderson et al. (2013). In a nutshell, we fit a Fourier series to model the phase-folded RV curve and increase the number of harmonics until an F-test indicates spurious fit improvement. This approach yields fit residuals that clearly exhibit a strong temporal correlation with an RMS of  $337 \text{ m s}^{-1}$ , see Fig. 3.

By running the fitting algorithm while assuming a model composed of the sum of a Fourier series and linear, quadratic, and cubic trends, we find that the orbital drift seen in *Hermes* RVs is best described by a cubic polynomial and that the best-fit pulsation model has 14 harmonics. We retain this model as our pulsation reference model for the following steps.

Figure 4 shows the residuals from *Hermes* RVs after subtracting the model that accounts for pulsations as well as the cubic drift due to orbital motion. The residuals are flat over the observational baseline. However, the phase-folded residuals do exhibit some structure, which is exposed by applying a color scale to trace the observation date. The RMS of our *Hermes* residuals is  $47 \text{ m s}^{-1}$ , i.e., higher than the  $18 \text{ m s}^{-1}$  estimated from RV standard stars in Sec. 2.1.

This higher-than-expected residual may be explained by small stochastic variations in the pulsation period seen in photometry of other Cepheids obtained with the *Kepler* and *MOST* satellites (so-called period-jitter, see Derekas et al. 2012; Evans et al. 2015), which



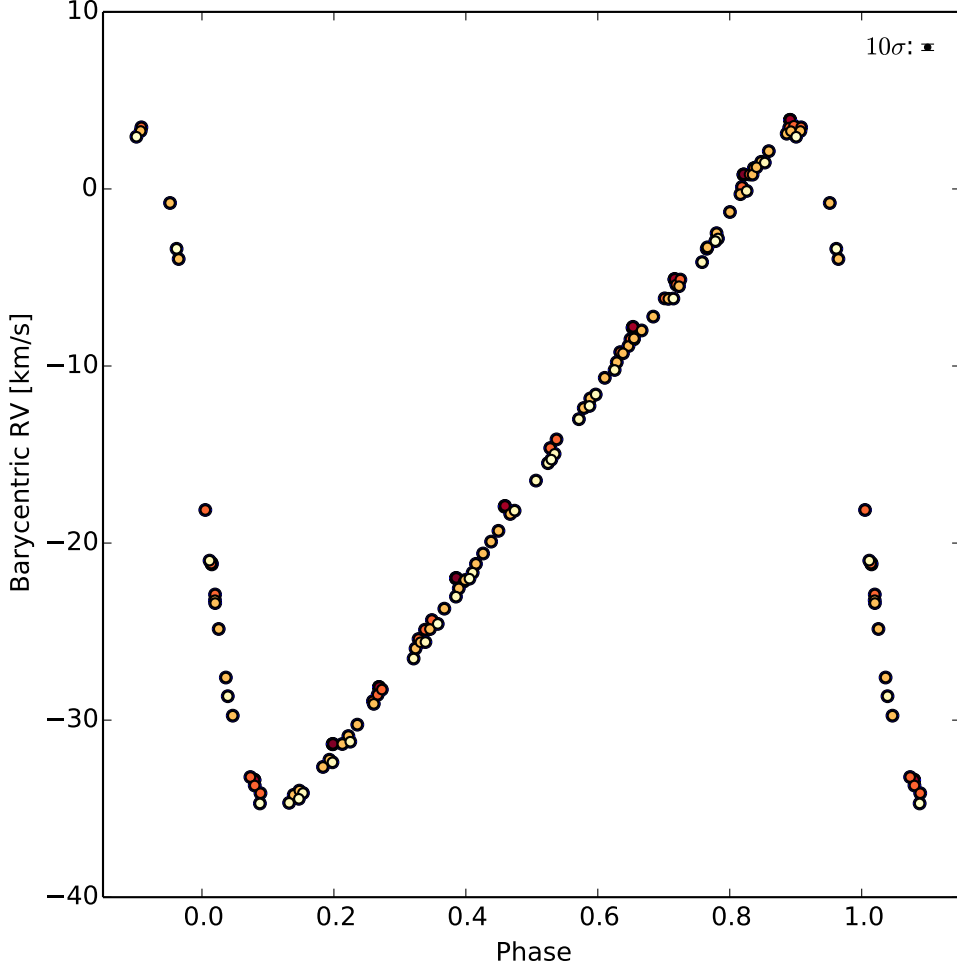


Fig. 2.— Phase-folded HERMES radial velocity curve with  $P_{\text{puls}} = 5.366274$  d. Observation date is traced by a color scale and increases from red to yellow. The ten-fold mean uncertainty of the measurements is shown in the top right corner. The RV offset at constant phase is due to the spectroscopic binary nature of  $\delta$  Cephei.

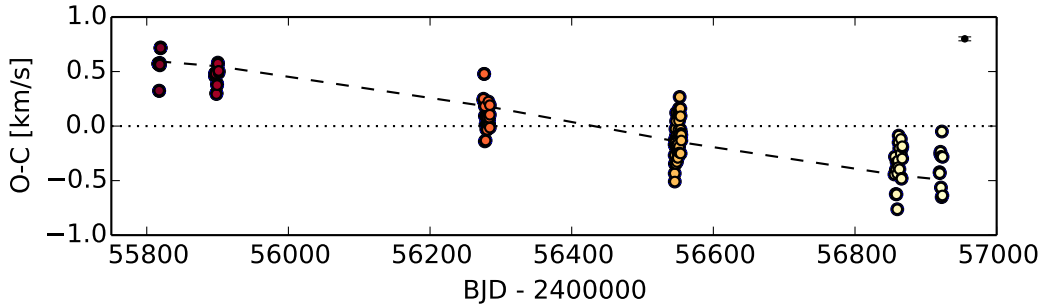


Fig. 3.— Residuals for *Hermes* RVs minus the pulsation model as a function of observation date. The trend (dashed line) reveals the presence of  $\delta$  Cephei’s spectroscopic companion.

has been explained as being due to surface convection and granulation (Neilson & Ignace 2014). We note also that Anderson (2014) recently discovered RV curve modulation in Cepheids, albeit at much lower amplitudes. Since these effects (period-jitter or modulation) limit our ability to precisely reproduce the pulsation curve, we adopt the RMS value of  $47 \text{ m s}^{-1}$  as our *Hermes* RV uncertainty for  $\delta$  Cephei for the remainder of our analysis.

### 3.2. Combination with literature data

The cubic drift seen in the residuals in Fig. 3 indicates orbital motion at a timescale longer than the observational baseline achieved by our *Hermes* observations. We therefore searched the literature for data suitable for determining the orbit of  $\delta$  Cephei.

$\delta$  Cephei is one of the most-studied variable stars and several authors have previously published RV data for it, including Shane (1958), Barnes et al. (1987), Wilson et al. (1989), Butler (1993), Bersier et al. (1994), Gorynya et al. (1996), Kiss (1998), Storm et al. (2004), Barnes et al. (2005). Historically,  $\delta$  Cephei’s RV curve has been thought to be well-understood, which may in part explain why its spectroscopic binary nature has gone unnoticed for so long. The main reason, however, is that  $\delta$  Cephei’s orbital signature has a small RV amplitude, high eccentricity, and long orbital period, and thus requires high-precision velocimetry over an observational baseline spanning at least two years. For comparison, the various RV datasets available in the literature have typical observational baselines on the order of one year and do not have sufficient precision to detect binarity during this timeframe.

Zero-point offsets must be corrected for when combining RV data from different instruments and the literature.  $\delta$  Cephei represents a particularly difficult case, because zero-point differences can be on the same order of magnitude as the difference in  $v_\gamma$  due to orbital motion between datasets. Therefore, a well-determined common zero-point is the key to determining the orbit of  $\delta$  Cephei accurately. To this end, we adopted the *CORAVEL-ELODIE* RV zero-point (cf. Udry et al. 1999a,b and Tab. 2).

Of the available literature sources, we excluded the following from our analysis due to insufficient precision ( $\sigma_{v_r} > 1 \text{ km s}^{-1}$ ): Shane (1958), Barnes et al. (1987), Wilson et al. (1989). We further discarded the measurements by Butler (1993) and Storm et al. (2004), since no information is available to determine the zero-point differences with *CORAVEL*. Finally, we excluded the single measurement published by Gorynya et al. (1996).

Conversely, the measurements published by Bersier et al. (1994) and Barnes et al. (2005),

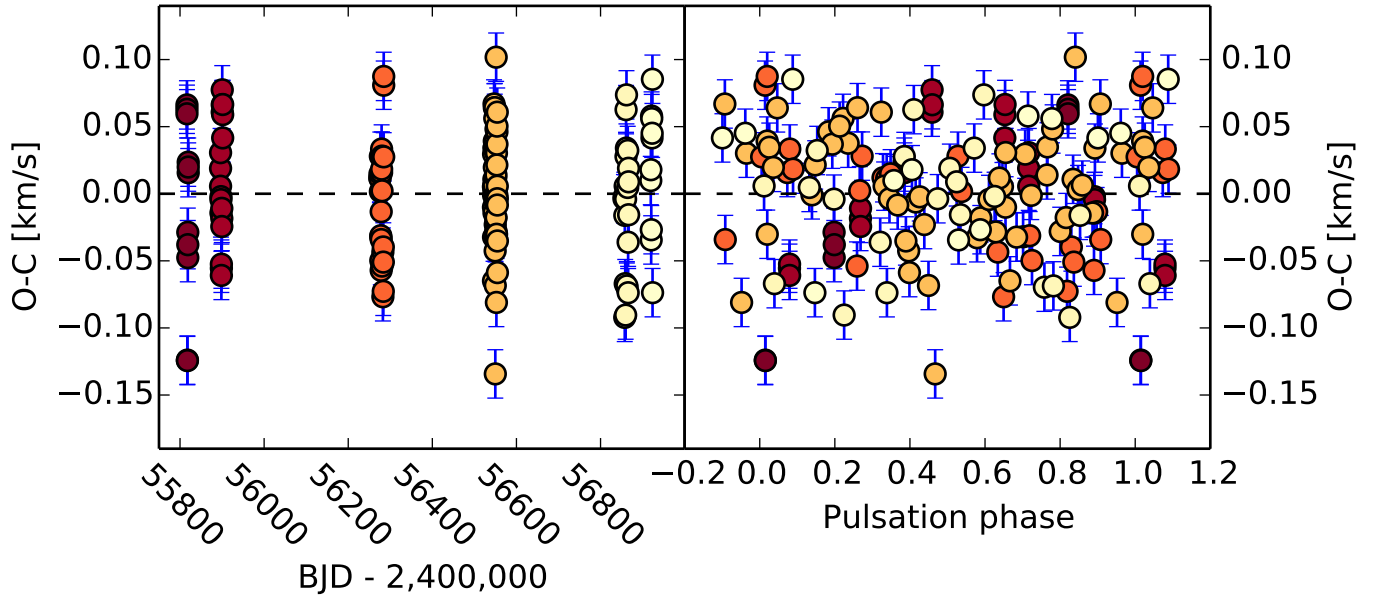


Fig. 4.— *Hermes* RV residuals ( $\text{RMS} = 47 \text{ m s}^{-1}$ ) after accounting for both pulsation and the cubic drift (see text) due to binarity. The left panel shows residuals as a function of the observation date, the right panel as a function of pulsation phase, with  $P_{\text{puls}} = 5.366274 \text{ d}$ . We trace observation date by color scaling the data points (red is oldest, yellow is newest) to expose additional signal that is not correctly modeled by pulsation and binarity and is likely related to random fluctuations in pulsation period (period-jitter).

as well as publicly available RV data from the *ELODIE* archive<sup>7</sup> (Moultaka et al. 2004) are already on the common *CORAVEL-ELODIE* RV zero-point. We found that an offset of  $-0.35 \text{ km s}^{-1}$  to the measurements by Kiss (1998) is appropriate to improve agreement with the (contemporaneous) data from the *ELODIE* archive and Barnes et al. (2005). This offset is similar to the precision stated by Kiss (1998,  $\sim 0.3 \text{ km s}^{-1}$ ). The determination of the zero-point offset between *Hermes* and *CORAVEL-ELODIE* is discussed in Sect. 3.1 above. Having thus calibrated the zero-point differences based on measurements of standard stars, we can use the combined data set to determine the orbit with confidence.

Classical Cepheids are known to exhibit changing periods due to their secular evolution. However, Cepheids can also exhibit erratic changes of unknown origin in their pulsation periods (see e.g. Berdnikov et al. 2000). When combining RV data from the literature, we noticed that variable periods have to be accounted for. We attempted to use the ephemerides and rate of (pulsation) period change by Berdnikov & Ignatova (2000) to obtain accurately phase-folded RV curves, but we were unable to obtain a satisfactory result.

Since obtaining good phase-folding is required in order to correctly subtract the pulsation reference model, we phase-folded the combined data set in the following way. First, we separated the dataset into three parts with different pulsation periods. The motivation for separating the evolution of the pulsation period in this way is the observation that the period of  $\delta$  Cephei changes very slowly (Eddington 1919, Berdnikov & Ignatova 2000). We then determined the best-fit pulsation periods for each of these three epochs by minimizing the scatter in the residuals after fitting for the pulsation alone. We thus adopt the following pulsation periods:  $5.3657 \pm 0.0013 \text{ d}$  for data by Bersier et al. (1994, mean epoch JD 2 444 467.12);  $5.36615 \pm 0.0005 \text{ d}$  for data from *ELODIE*, Kiss (1998), and Barnes et al. (2005, mean epoch JD 2 450 398.61);  $5.366274 \pm 0.00006 \text{ d}$  for *Hermes* RVs (mean epoch JD 2 456 430.38). While the center values of this sequence would imply a slowly increasing pulsation period ( $dP/dt \sim 0.5 - 1.1 \times 10^{-5} \text{ yr}^{-1}$ ), these adopted periods agree to within their uncertainties. After applying our updated pulsation periods, we shifted all three epochs for  $\phi \equiv 0$  to occur at minimum radius, i.e., when the velocity is equal to  $v_\gamma$  on the steep part of the RV curve. This provides us with an accurately phase-folded pulsation curve from which we subtract the pulsation reference model to reveal the orbital motion of  $\delta$  Cephei.

Figure 5 shows the RV curve based on the combined dataset. The residuals clearly demonstrate the presence of orbital motion.

---

<sup>7</sup><http://atlas.obs-hp.fr/elodie/>

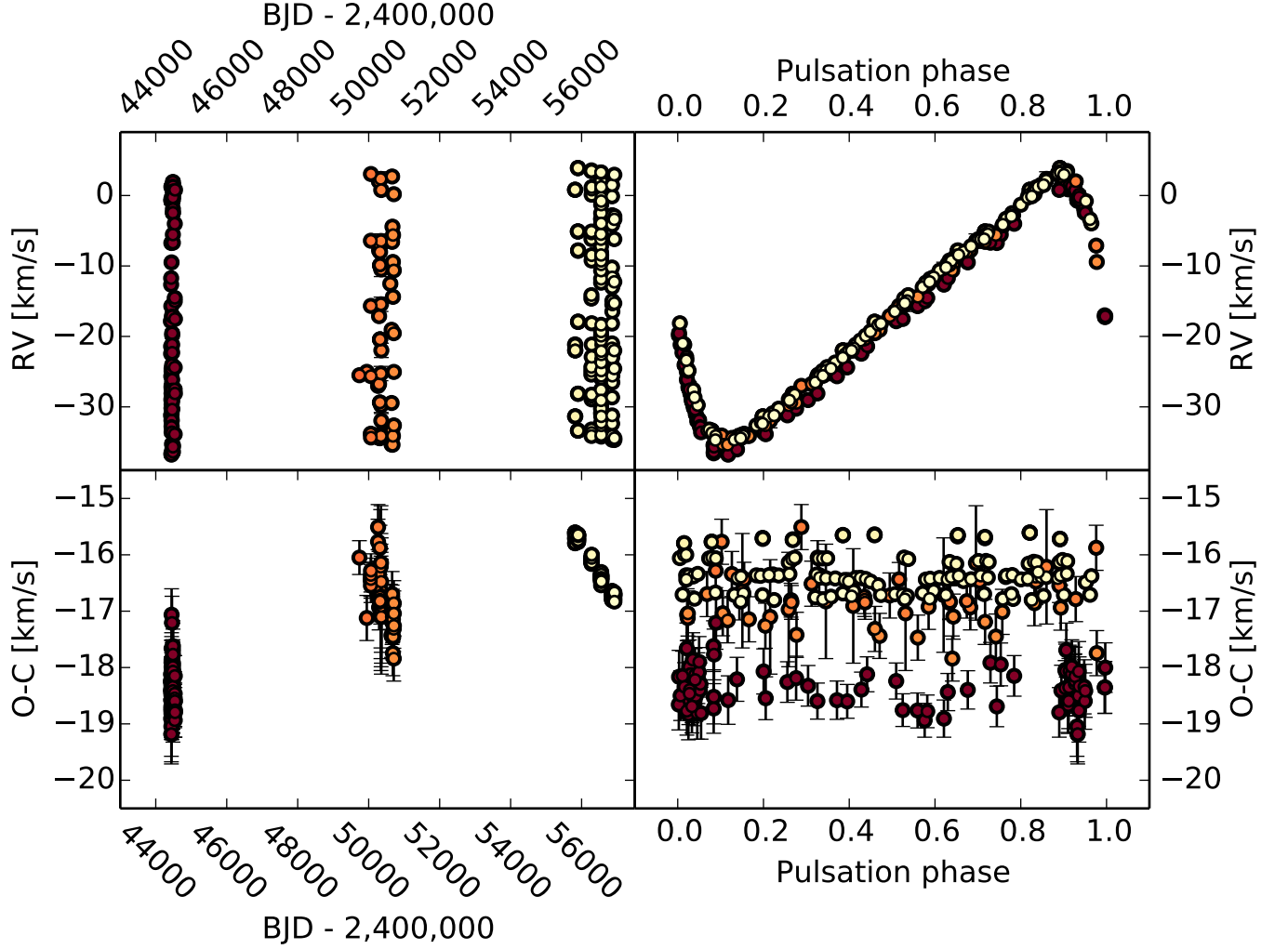


Fig. 5.— The combined dataset (*Hermes* + literature RVs) modeled only for pulsation-induced variability. The left panels show the measurements (top) and residuals (bottom) against observation date, the right hand panels show the same measurements against pulsation phase. Observation date is traced by the applied color scale, with the newest measurements drawn white.

### 3.3. Orbit Determination using HERMES and Literature RVs

Figure 6 shows the orbital motion of  $\delta$  Cephei exposed by subtracting our pulsation reference model from the phase-folded combined dataset. As can be seen in the top right panel, the orbit is well-sampled except for the ascending part of the orbital RV curve. Our observations did not sample this part of the RV curve, since it occurred shortly (a few months) before the start of our observations.

Table 3 provides the orbital solution for  $\delta$  Cephei determined from the orbit-only combined RV curve using a standard Keplerian model. We used the tool *Yorbit* (Ségransan, et al., in prep.) to first determine an initial orbital estimate via a genetic algorithm and then characterize the parameter uncertainties using the marginal distributions of Markov Chain Monte Carlo simulations with 500 000 iterations, cf. Fig. 7. From the orbital solution and assuming  $M_{\delta\text{Cep}} \sim 5.0 - 5.25 M_{\odot}$  (cf. Sec. 6) we determine the minimum mass of the companion to be  $0.2 \pm 0.02 M_{\odot}$ . While  $a_{\text{rel}}$  and  $a_1 \sin i$  are listed assuming  $M_{\delta\text{Cep}} = 5.25 M_{\odot}$ , the stated values remain within the stated uncertainties if  $M_{\delta\text{Cep}} = 5.0 M_{\odot}$  is adopted.

Comparing our results to other known Cepheid orbits listed in the Cepheid binary database by Szabados (2003), we find that the semi-amplitude  $K$  of this orbit is the second smallest among all known binary Cepheid orbits, albeit with much larger eccentricity and somewhat longer period than W Sgr’s orbit (Groenewegen 2008). This also helps to explain why  $\delta$  Cephei has not previously been identified as a spectroscopic binary.

## 4. Searching for an Astrometric Orbital Signature

Projecting the orbit derived in Sect. 3.3 to the distance determined by Benedict et al. (2007,  $\varpi = 3.66 \pm 0.15$  mas) yields an orbital relative semimajor axis of  $a_{\text{rel}} = 21.2$  mas, with

| Parm       | $v_{\gamma}$          | $T_0$              | $P_{\text{orb}}$ | $K$                   | $e$   | $\omega$ | $a_{\text{rel}}$ | $a_1 \sin i$          | $f_m$                           |
|------------|-----------------------|--------------------|------------------|-----------------------|-------|----------|------------------|-----------------------|---------------------------------|
| Unit       | [km s <sup>-1</sup> ] | [d]                | [d]              | [km s <sup>-1</sup> ] |       | [deg]    | [au]             | [10 <sup>-3</sup> au] | [10 <sup>-3</sup> $M_{\odot}$ ] |
| Value      | -16.787               | 55649.68           | 2201.87          | 1.509                 | 0.674 | 246.77   | 5.82             | 226.3                 | 0.784                           |
| $\sigma_+$ | 0.026                 | 24.68 <sup>†</sup> | 5.73             | 0.239                 | 0.038 | 2.37     | 0.18             | 21.9 <sup>†</sup>     | 0.249 <sup>†</sup>              |
| $\sigma_-$ | 0.049                 | 19.86 <sup>†</sup> | 6.31             | 0.080                 | 0.021 | 4.90     | 0.19             | 7.9 <sup>†</sup>      | 0.083 <sup>†</sup>              |

Table 3: Orbital solution for  $\delta$  Cephei based on the combined *Hermes* and literature radial velocities.  $\sigma_+$  and  $\sigma_-$  denote the upper and lower standard errors derived from marginal distributions. Quantities with superscript dagger have been computed using Gaussian error propagation. Other uncertainties were estimated by the MCMC analysis.

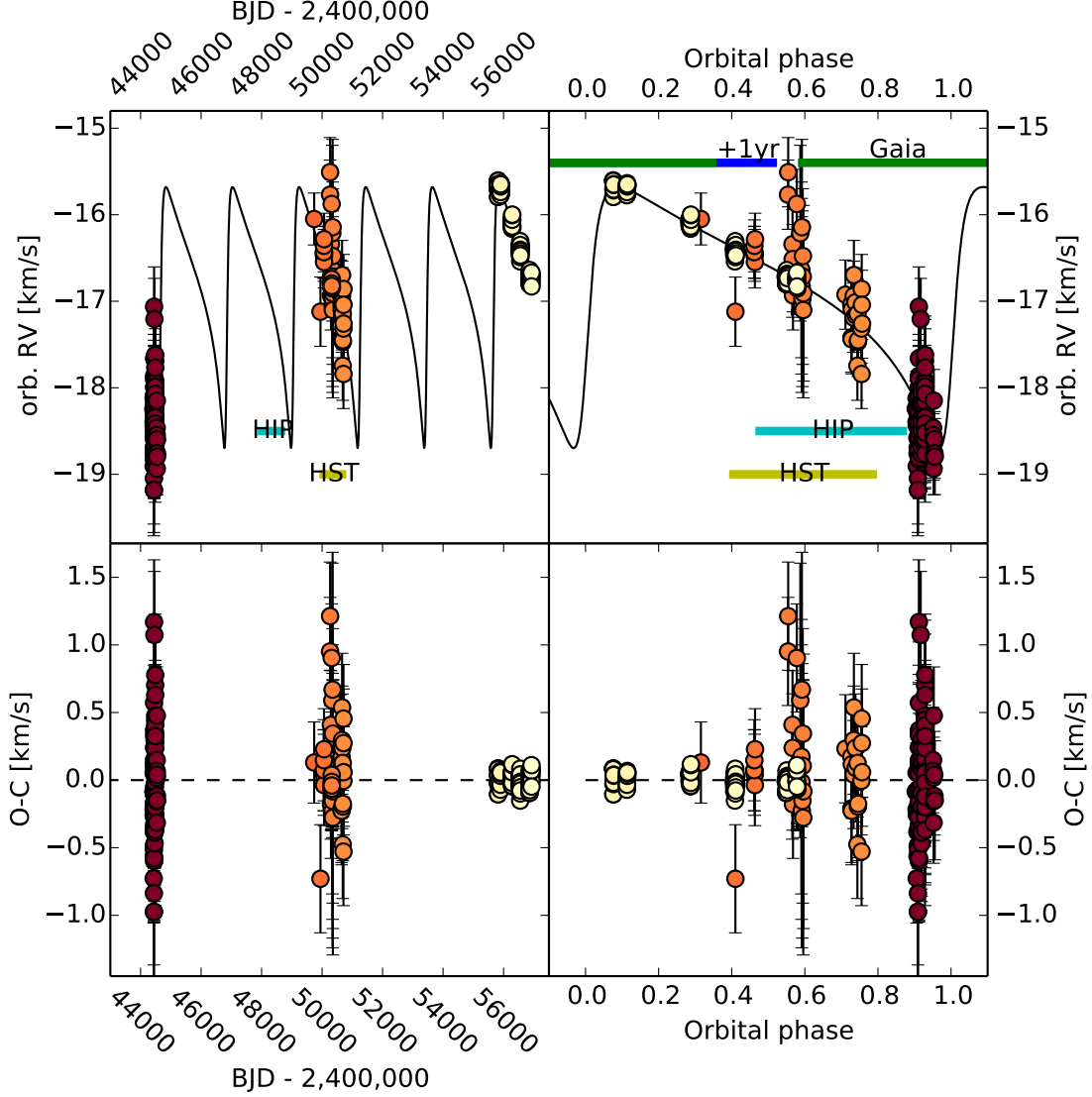


Fig. 6.— Orbital solution for  $\delta$  Cephei based on the combined dataset from which we subtracted our pulsation reference model. We trace observation date by color scaling data points from red for the oldest to yellow for the newest measurements. Left panels show measurements (top) and residuals (bottom) against observation date, right panels show the same data against orbital phase, assuming  $P_{\text{orb}} = 2201.87$  d, see Tab. 3, and  $\phi \equiv 0$  at pericenter passage. We indicate the range of orbital phases at which *Hipparcos*, *HST*, and *Gaia* have observed or will observe  $\delta$  Cephei.

an orbital barycentric semimajor axis of the Cepheid of  $a_1 > 0.84 \text{ mas}$ , a value more than five times the uncertainty estimated by Benedict et al. (2007), and even seven times the uncertainty stated by van Leeuwen et al. (2007, *Hipparcos*,  $3.71 \pm 0.12 \text{ mas}$ ). This prompts the question whether the observations taken by *Hipparcos* or *HST* are sensitive to the orbital motion, cf. Fig. 6 for information as to which ranges of orbital phase were observed by these missions. We therefore explore the sensitivity of *Hipparcos* and *Gaia* astrometry to  $\delta$  Cephei’s hidden companion in this section.

#### 4.1. Hipparcos Intermediate Astrometric Data

To test whether *Hipparcos* (Perryman & ESA 1997) was sensitive to the orbital motion of  $\delta$  Cephei, we analyze the *Hipparcos* intermediate astrometric data (IAD) published on the DVD attached to the new reduction by van Leeuwen (2007).

##### 4.1.1. Parallax from Intermediate Astrometry Data

A 5-parameter fit to the 95 measurements given on the DVD yields the residuals shown in Fig. 8, left panel. There are several outliers and fit quality is poor ( $\chi_{\text{red}}^2 = 2.01$ ,  $\text{RMS}(\text{O}-\text{C}) = 1.43 \text{ mas}$ ). We obtain a best fit parallax of  $\varpi_{\text{all}} = 4.37 \pm 0.27 \text{ mas}$ .

We therefore discarded a total of 6 data points on the basis of their excess residual from the following satellite orbits: 180, 252, 396, 759, 1786, and 2126. We then repeated the 5-parameter fit to 89 measurements and obtained a better fit (Fig. 8, right panel;  $\chi_{\text{red}}^2 = 0.65$ ,  $\text{RMS}(\text{O}-\text{C}) = 0.81 \text{ mas}$ ), as well as smaller parallax:  $\varpi_{5\text{parm}} = 4.09 \pm 0.16 \text{ mas}$ . Note that

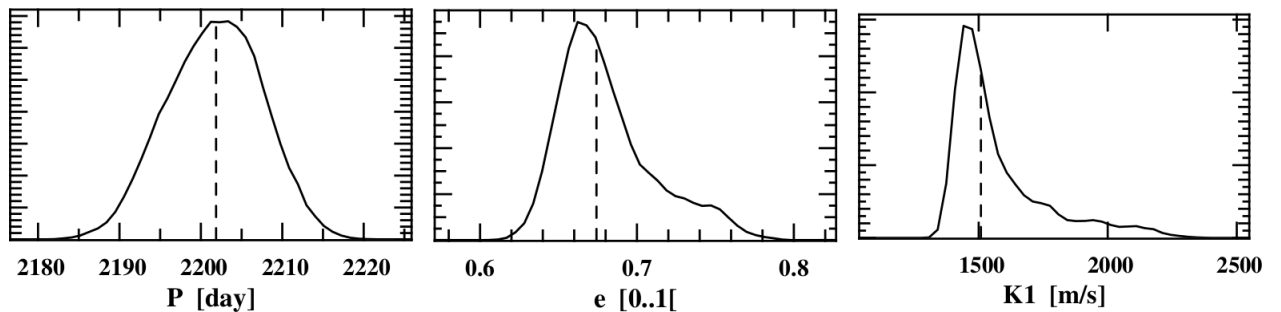


Fig. 7.— Marginal probability density functions for orbital period, eccentricity, and semi-amplitude as determined by *Yorbit*’s MCMC algorithm. The dashed line indicates the median value adopted as numerical reference.



there is a discrepancy of  $\Delta\varpi = 0.38$  mas (0.21 mag) between the parallax value published in the van Leeuwen (2007,  $\varpi = 3.77 \pm 0.16$  mas) reduction and our result based on the IAD. There may be several reasons for such a discrepancy, including:

1. Our fitting routine. We excluded this possibility by processing other stars, in particular  $\delta$  Cephei’s visual companion HD 213307 for which we obtained a parallax of  $3.69 \pm 0.46$  mas in exact numerical agreement with the published value ( $3.69 \pm 0.46$  mas, van Leeuwen 2007). As an additional cross-check, we applied the same methodology to more than 20 other Cepheids using the same routine and obtained results that agree well with the published values of van Leeuwen (2007).
2. our selection of IAD. As noted in the IAD header, 3% of the IAD were discarded to obtain the solution of van Leeuwen (2007), although it is not specified which ones. We attempted to reproduce their result by discarding only 3 measurements but did not succeed.
3. the cluster solution. It appears that van Leeuwen (2007) used a special procedure for cluster stars to better remove outlier measurements for individual stars, under the assumption that all cluster stars are at indistinguishable distance. While our parallax result is larger than the previously published value, it is well within the wide range of parallaxes ( $2.57 - 5.28$  mas) reported for presumed members of Cep OB6.
4. other unknown procedures or modifications that may have been applied specifically to  $\delta$  Cephei’s parallax to achieve the solutions presented by van Leeuwen (2007) and van Leeuwen et al. (2007).

Our parallax estimate ( $\varpi = 4.09 \pm 0.16$  mas) is also considerably ( $2\sigma$ ) larger than the *HST*-based result by Benedict et al. (2002,  $\varpi = 3.66 \pm 0.15$  mas). Such an increase in parallax would increase  $\delta$  Cephei’s absolute magnitude by 0.24 mag, making it intrinsically fainter than previously thought ( $M_V = -3.23$  mag using the absolute magnitude published by Benedict et al. 2002). We note that the *HST*-based period-luminosity relations presented by Benedict et al. (2007) seem to agree better with such an increase in absolute magnitude for  $\delta$  Cephei.

The *HST* observations were taken at an orbital phase at which a significant parallax bias due to orbital motion is not very likely, cf. Fig. 6. However, the assumption of a physical association between HD 213307 as well as  $\delta$  Cephei in the loose association Cep OB6 was required to “reduce [the *HST*] astrometric residuals to near-typical levels” (Benedict et al. 2002, Sec. 5.5).

Concerning  $\delta$  Cephei’s membership in Cep OB6, we note that the association’s discovery did not take into account radial velocity data, since only little such information was available at the time (de Zeeuw et al. 1999). Inspection of the **SIMBAD** database yields radial velocity information for 10 of the 19 presumed member stars (in addition to  $\delta$  Cephei), with values ranging from  $-7 \text{ km s}^{-1}$  to  $-38 \text{ km s}^{-1}$  and median uncertainty of  $1.2 \text{ km s}^{-1}$  based on measurements by: Fehrenbach et al. (1996); Grenier et al. (1999); Famaey et al. (2005); Gontcharov (2006); Kharchenko et al. (2007). The RVs are distributed as follows: HIP110807 and HIP112998 have  $v_r \sim -7 \pm 2 \text{ km s}^{-1}$ , HIP110497 has  $v_r = -13.3 \pm 0.5 \text{ km s}^{-1}$ , HIP109492 and HIP110988 (= HD213307) are close to  $\delta$  Cephei’s  $v_\gamma = -16.8 \text{ km s}^{-1}$  (to within  $1 \text{ km s}^{-1}$ ), HIP113993 has  $v_r = -20.9 \pm 1.1 \text{ km s}^{-1}$ , HIP113316 has  $v_r = -25.6 \pm 8 \text{ km s}^{-1}$ , and three stars (HIP110266, HIP110275, HIP110356) have  $v_r < -30 \text{ km s}^{-1}$  with reported uncertainties between 3 and  $15 \text{ km s}^{-1}$ . This relatively wide range of RVs suggests that Cep OB6 is not gravitationally bound<sup>8</sup>, i.e. that the assumption of a common distance for all presumed member stars is not valid. This interpretation is corroborated by the wide range of parallax values of the presumed member stars (see item 3 above). However, more homogeneous and high-quality radial velocity measurements of the presumed members of Cep OB6 are required to further illuminate this issue.

Although the above suggests that not all of Cep OB6’s presumed members have indistinguishable distance, we note that the observational evidence does support the physical association between HD 213307 and  $\delta$  Cephei, since their parallaxes and radial velocities agree to within the uncertainties. A re-assessment of the *HST* astrometric data without the assumption of cluster membership (this affects e.g. the spectrophotometric parallax for HD 213307, which is part of the *HST* reference frame), and taking into account  $\delta$  Cephei’s orbital motion would be useful for testing whether the difference between the published *HST* parallax and our result can be reconciled.

#### 4.1.2. Orbit Analysis

We search for an orbital signature in *Hipparcos* IAD using the methodology described in Sahlmann et al. (2011b), which has been shown to reliably detect such orbital signatures in *Hipparcos* IAD (Sahlmann et al. 2011b,a; Sahlmann & Fekel 2013). We use the spectroscopic orbital parameters given in Tab. 3 to fit the IAD with a seven-parameter model, which has the free parameters inclination  $i$ , longitude of the ascending node  $\Omega$ , parallax  $\varpi$ , and offsets

---

<sup>8</sup>For this to be the case, the RV dispersion of member stars should not exceed a few  $\text{km s}^{-1}$  (e.g. Mathieu 1986).

to the coordinates  $(\Delta\alpha, \Delta\delta)$  as well as offsets to the proper motions  $(\Delta\mu\alpha, \Delta\mu\delta)$ . We then search a two-dimensional grid in  $i$  and  $\Omega$  for its global  $\chi^2$ -minimum with a nonlinear minimization procedure. We determine the statistical significance of the derived astrometric orbit via a permutation test (Zucker & Mazeh 2001) for which we employ 1000 pseudo-orbits and derive parameter uncertainties using Monte Carlo simulations that include propagation of RV parameter uncertainties.

Only 41% of the orbit are probed by *Hipparcos* measurements, whose average measurement uncertainty of 1.07 mas is furthermore greater than the barycentric minimum semimajor axis of the orbit (0.84 mas). It may therefore not surprise that we determine virtually identical results for 5-parameter (single star) and 7-parameter (binary) models, with flat residuals even for the 5-parameter model (Fig. 8). From an F-test, we obtain a probability of 4.4% that the single-star model is true, and the permutation test yields an orbit detection significant at the  $1.8\sigma$  level (93.7%). While the evidence for the orbital signature is only marginally significant, it has been determined with two independent methods that are in agreement. It thus appears that there is some temporal coherence present in the *Hipparcos* data, although we cannot claim orbit detection using *Hipparcos* astrometry. We can, however, use our orbital analysis to set (very) loose constraints on the inclination ( $10^\circ \lesssim i \lesssim 170^\circ$ ) of the orbit, see Fig. 9, allowing us to place an upper limit on the companion mass with  $0.2 M_\odot \lesssim M_2 \lesssim 1.2 M_\odot$ , which is fully consistent with the lack of spectral features due to the companion in the *Hermes* data set, cf. Sect. 3.

While we are unable to claim detection of the orbit from *Hipparcos* astrometric data, we caution that the previous estimate of  $\delta$  Cephei’s proper motion may have been affected by the companion.

## 4.2. Gaia

The *ESA* space mission *Gaia*<sup>9</sup> is currently conducting an unprecedented census of our Galaxy, measuring position, proper motion, and parallax for more than a billion stars during a nominal mission duration of five years.  $\delta$  Cephei will be among these billion objects thanks to *Gaia*’s ability to observe very bright stars<sup>10</sup> (Martín-Fleitas et al. 2014). For an assumed single-measurement precision of  $\sigma_{\text{Gaia}} \approx 100 \mu\text{as}$ , the minimum barycentric semimajor axis ( $a_1 \sin i \approx 840 \mu\text{as}$  (Sect. 3.3)) is roughly 8 times larger than the measurement uncertainty.

---

<sup>9</sup><http://www.cosmos.esa.int/web/gaia>

<sup>10</sup>Stars brighter than  $G$ -band magnitude 5.7 will be heavily saturated and need special treatment to determine their centroids. We conservatively assume a single observation per *Gaia* field-of-view transit.

Figure 6 shows the range of orbital phases covered during the nominal mission duration plus a possible one year extension. It shows that *Gaia* measurements will cover the majority of the orbit and, crucially, will be measuring astrometry during periastron passage. We investigate the detectability of  $\delta$  Cephei’s orbit from *Gaia* astrometry in two ways.

First, the detectability of astrometric orbits with *Gaia* can be estimated from a consideration of the astrometric signal-to-noise  $S/N = a_1 \sqrt{N}/\sigma_{\text{Gaia}}$  (Sahlmann et al. 2011a, 2015). Assuming 86 *Gaia* observations of  $\delta$  Cephei during the 5-year mission (see below) and accounting for 10% dead time with an assumed  $100 \mu\text{as}$  accuracy for individual measurements and the minimum amplitude of  $\sim 840 \mu\text{as}$ , we obtain  $S/N \approx 73$ , which is much higher than the detection threshold of 20 described in Sahlmann et al. (2015). This indicates that *Gaia* will detect the astrometric orbit of  $\delta$  Cephei, despite not measuring at all orbital phases.

Second, we use the *Gaia* astrometric simulation software **AGISlab** (Holl et al. 2012) to investigate the detectability of  $\delta$  Cephei’s orbit derived in Sect. 3.3. We adopt the  $\Delta\chi^2$  metric from Perryman et al. (2014) to evaluate the detectability of the astrometric binary signal. This metric measures the reduction in minimum  $\chi^2$  when going from a (single-star) 5-parameter solution to a (binary) 12-parameter Keplerian solution. Even for our adopted worst-case scenario<sup>11</sup>, we find an improvement of  $\Delta\chi^2_{\text{min},3\sigma} = 139$  when accounting for the orbital motion. This is well above the threshold for precise (parameters determined to better than 10%) orbit characterization (Perryman et al. 2014,  $\Delta\chi^2 > 100$ ). We therefore predict that *Gaia* will clearly detect and characterize the astrometric counterpart to the spectroscopic orbit discovered here.

## 5. Discussion: Piecing Together the Puzzle

Now that  $\delta$  Cephei’s nature as a spectroscopic binary is revealed, it is worth revisiting other observed features of the prototype of classical Cepheids in this new light.

Engle et al. (2014) recently provided evidence that  $\delta$  Cephei is a soft X-ray source with a luminosity of  $L_X(0.3-2\text{keV}) \approx 4.5-13 \times 10^{28} \text{ erg s}^{-1}$  and peak flux at  $kT = 0.6-0.9 \text{ keV}$ . As these authors discuss, young ( $\sim 120 \text{ Myr}$  for a  $5 M_\odot$  Cepheid, according to Geneva evolution models by Ekström et al. 2012; Georgy et al. 2013) low-mass main-sequence companions can provide coronal X-ray emission. In Sects. 3.3 and 4.1.2, we constrained the mass range for the unseen companion to be  $0.2 < M_2 < 1.2 M_\odot$  based on radial velocities and *Hipparcos*

---

<sup>11</sup>This assumes the worst possible configuration of sky-alignment and observation noise, as well as 20% dead time

astrometric measurements. As Cepheids are rarely detected in X-rays, it appears likely that  $\delta$  Cephei’s young main sequence companion is responsible for the detected variable X-ray activity.

Due to the high eccentricity of the orbit,  $\delta$  Cephei and its companion have recurrent close encounters, with a pericenter distance of  $r_{\text{per}} = (1-e)a_{\text{rel}} = 1.89 \text{ au} = 409 R_{\odot} = 9.5 R_{\star}$ , where  $R_{\star} = 43.3 R_{\odot}$  (Turner 1988; Mérand et al. 2005; Natale et al. 2008). It is also important to bear in mind that  $\delta$  Cephei is currently in the core He burning phase, most likely on the second crossing of the instability strip as shown by the decrease in pulsation period (measured e.g. by E. Hertzsprung and reported by Eddington 1919, Berdnikov & Ignatova 2000, and Engle et al. 2014). It has therefore previously occupied the red giant branch, where its radius was even larger, approximately  $R_{\star, RG} \sim 80 R_{\odot}$ . Assuming an unchanged orbit, pericenter passage would have brought the two stars to within  $5 \times R_{\star, RG}$ .

Taking these considerations further, we consider the possibility of previous interactions between  $\delta$  Cephei and its companion. Since  $\delta$  Cephei is on a highly eccentric orbit and the Roche-lobe formalism is valid only for circular orbits, we adopt the Roche-lobe formalism in the quasi-static approximation as presented by Sepinsky et al. (2007a). Assuming  $M_{\delta \text{ Cep}} = 5.2 M_{\odot}$ ,  $M_2 = 0.7 M_{\odot}$ , and equatorial velocity  $v_{eq} = 10 \text{ km s}^{-1}$ , we obtain the volume-equivalent Roche lobe radius at pericenter of  $R_{\text{Roche, corr}} = 1.05 \text{ au} \approx 5.2 R_{\star} \approx 2.8 R_{\star, RG}$ . Hence, at pericenter passage  $\delta$  Cephei fills 19% of its (quasi-static) Roche lobe, and the Roche lobe radius at pericenter is approximately 55% of the distance at pericenter passage ( $r_{\text{per}} = 1.89 \text{ au}$ ). At apocenter, the distance between the two stars is a factor  $(1+e)/(1-e) = 5.1$  larger, and  $\delta$  Cephei fills only about 3.7% of its Roche lobe.  $\delta$  Cephei may thus become noticeably deformed due to tidal interactions close to pericenter passage, while being spherical near apocenter passage. During the red giant phase, this situation would have been even more extreme, if the past orbit was similar to the present-day orbit. The above considerations suggest that the observed circumstellar material (Marengo et al. 2010; Mérand et al. 2006) and bow-shock (Matthews et al. 2012) may originate from previous and ongoing binary interactions. A more detailed investigation of such interactions is required to discuss this scenario in terms of  $\delta$  Cephei’s mass loss history (see the discussion in Matthews et al. 2012), but is considered out of scope for this paper.

If  $\delta$  Cephei and its companion have a history of episodal interactions at pericenter passage, then the high eccentricity of the orbit may appear surprising. However, Sepinsky et al. (2007b) showed that rapid circularization is not expected for all close-in binaries with this type of interactions. Applying our results for  $\delta$  Cephei to their formalism shows that  $\delta$  Cephei’s orbit is not expected to have been rapidly circularized. Furthermore,  $\delta$  Cephei is a visual binary whose outer companion is understood to be physically associated and on a

very long-period orbit (Benedict et al. 2002). The high eccentricity of the inner binary (the one shown in the present work) could thus have been driven up by the outer companion by a Kozai-Lidov mechanism (Lidov 1962; Kozai 1962) and may have varied significantly over its evolutionary history.

If  $\delta$  Cephei and its companion have undergone significant interactions, one might expect the evolutionary status of  $\delta$  Cephei to vary significantly from that of a Cepheid with a single star progenitor. We therefore examine  $\delta$  Cephei’s current evolutionary status in Figure 10 to search for signs of non-standard evolution. We compare observed absolute  $V$  magnitude,  $(B - V)_0$  color (both from Benedict et al. 2002), and rate of (pulsation) period change  $\dot{P}_{\text{puls}} = -0.1006 \pm 0.0002$  (Engle et al. 2014) with predictions from Geneva stellar evolution models<sup>12</sup> of Solar metallicity that include rotation (Ekström et al. 2012; Georgy et al. 2013) and have been studied specifically in the context of classical Cepheids by Anderson et al. (2014). Strong disagreement between the observations and these predictions could be considered evidence for binary interactions, since no binary interactions are accounted for in these model predictions. However, we find that  $\delta$  Cephei’s location in both diagrams is consistent with a  $5.25 M_{\odot}$  Cepheid whose progenitor had a slightly faster-than-average initial rotation ( $\Omega/\Omega_{\text{crit}} \sim 0.7$ ). Assuming these parameters for the evolutionary models yields an age of 112 Myr. Adopting our new parallax from Sec. 4.1.1 yields a smaller initial mass of  $M \approx 5.0 M_{\odot}$  and thus an older age of 127 Myr, while leaving the implications regarding the rotational history unchanged.

At the present level of accuracy, we thus do not find any irreconcilable discrepancies between the predicted and observed evolutionary states of  $\delta$  Cephei. This shows that binary interactions, if present, have either had a negligible effect on the evolutionary path of  $\delta$  Cephei, or that the interactions are weak and slow enough for  $\delta$  Cephei to reach an equilibrium state similar to a non-interacting star.

In summary, the discovery of  $\delta$  Cephei’s nature as a spectroscopic binary helps to complete the puzzle created by a plethora of observations. While there is no clear evidence for a non-standard evolutionary path,  $\delta$  Cephei is a particularly interesting example of the limitations that this evolutionary phase is subject to for binary stars (cf. Neilson et al. 2014) and deserves detailed observational follow up and dynamical modeling to further investigate its intriguing past that may have been marked by tidal interactions due to both the inner (discovered here) and outer (HD 213307) companions.

---

<sup>12</sup>Models accessible at <http://obswww.unige.ch/Recherche/evoldb/index/Interpolation/>

## 6. Conclusions

230 years after the discovery of its variability (Goodricke 1786), we discover the spectroscopic binary nature of  $\delta$  Cephei, archetype of classical Cepheid variable stars and one of the most-studied variable stars.

Our discovery is demonstrated using new high-precision radial velocities measured from high-quality optical spectra obtained with the high-resolution spectrograph *Hermes*. Combining these new high-precision data with lower-precision RVs from the literature, we determine the orbital solution for the spectroscopic binary, which is an inner binary to the outer visual binary system discussed by Benedict et al. (2002).  $\delta$  Cephei thus appears to be a pair of binary stars.

We re-analyze *Hipparcos* intermediate astrometric data (cf. Sects. 4.1.1) and obtain the parallax  $\varpi = 4.09 \pm 0.16$  mas ( $d = 244 \pm 10$  pc) using a 5-parameter (single star) model. This result is larger than the estimates reported by van Leeuwen (2007,  $\varpi = 3.77 \pm 0.16$  mas), van Leeuwen et al. (2007,  $\varpi = 3.71 \pm 0.12$  mas), and Benedict et al. (2002,  $3.66 \pm 0.15$  mas). While these previously published results based on *Hipparcos* and *HST* astrometry agree to within their stated uncertainties, they all shared a common assumption of  $\delta$  Cephei’s membership in the loose association Cep OB6, which our analysis does not and which we argue should be revisited using radial velocities. Relaxing this assumption and accounting for orbital motion in a re-analysis of the *HST* astrometric data would be useful to test whether the existing *HST* astrometry can be reconciled with our *Hipparcos*-based result.

We perform an orbital analysis of the *Hipparcos* IAD in Sect. 4.1.2 and find tentative evidence for an orbital signature, although no detection can be claimed. Based on detailed simulations, we show that *Gaia* is highly sensitive to the astrometric orbit of  $\delta$  Cephei and will likely model the full set of Keplerian parameters with better than 10% accuracy. The orbit will have to be accounted for when determining proper motions from *Hipparcos* and *Gaia* data.

Using the constraints provided by the optical spectra, the orbit measured from RVs, the astrometric orbital analysis, and assuming a mass of  $5.0 - 5.25 M_{\odot}$ , we constrain the mass range of the companion to be  $0.2 < M_2 < 1.2 M_{\odot}$ . Adopting the lower mass for  $\delta$  Cephei mainly affects the upper mass limit, which would become  $1.1 M_{\odot}$  in this case. Given that the spectroscopic companion is expected to be the same age as  $\delta$  Cephei, i.e., approximately 100–130 Myr (depending on mass and ZAMS rotation rate of the progenitor), the reported X-ray emission detected using *XMM-Newton* (Engle et al. 2014) could be explained by magneto-rotational activity of a young main-sequence star.

The close periastron approach of the two stars has potentially far-reaching consequences

for the explanation of the observed circumstellar environment of  $\delta$  Cephei. Detailed modeling of the orbital and stellar evolution of this complex system is desirable to further improve our understanding of the archetype of classical Cepheids and its intriguing past.

Many thanks are due to everyone who aided in securing the analyzed datasets and, in particular, to the *Hermes* and *Mercator* teams. Damien Ségransan is acknowledged for assistance regarding the use of *Yorbit*. RIA acknowledges Miranda A. Gaanderse for her creative assistance in finding the title for this paper and Dr. Paul I. Anderson for his careful reading of the manuscript. We thank the anonymous referees for their constructive reports.

This research is based on observations made with the Mercator Telescope, operated on the island of La Palma by the Flemish Community, at the Spanish Observatorio del Roque de los Muchachos of the Instituto de Astrofísica de Canarias. *Hermes* is supported by the Fund for Scientific Research of Flanders (FWO), Belgium, the Research Council of K.U. Leuven, Belgium, the Fonds National de la Recherche Scientifique (F.R.S.-FNRS), Belgium, the Royal Observatory of Belgium, the Observatoire de Genève, Switzerland, and the Thüringer Landessternwarte, Tautenburg, Germany. This study also employed spectral data retrieved from the *ELODIE* archive at Observatoire de Haute-Provence (OHP).

This research has made use of NASA’s ADS Bibliographic Services, the SIMBAD database and the VizieR catalogue access tool provided by CDS, Strasbourg, and Astropy, a community-developed core Python package for Astronomy (Astropy Collaboration et al. 2013).

RIA acknowledges funding from the Swiss NSF. JS is supported by an ESA research fellowship in space science.

## REFERENCES

- Anderson, R. I. 2013, PhD thesis, Université de Genève
- Anderson, R. I. 2014, A&A, 566, L10
- Anderson, R. I., Ekström, S., Georgy, C., et al. 2014, A&A, 564, A100
- Anderson, R. I., Eyer, L., & Mowlavi, N. 2013, MNRAS, 434, 2238
- Astropy Collaboration, Robitaille, T. P., Tollerud, E. J., et al. 2013, A&A, 558, A33
- Baade, W. 1926, Astronomische Nachrichten, 228, 359



- Baranne, A., Queloz, D., Mayor, M., et al. 1996, *A&AS*, 119, 373
- Barnes, III, T. G., Jeffery, E. J., Montemayor, T. J., & Skillen, I. 2005, *ApJS*, 156, 227
- Barnes, III, T. G., Moffett, T. J., & Slovak, M. H. 1987, *ApJS*, 65, 307
- Belopolsky, A. 1894, *Astronomische Nachrichten*, 136, 281
- Belopolsky, A. 1895, *ApJ*, 1, 160
- Benedict, G. F., McArthur, B. E., Feast, M. W., et al. 2007, *AJ*, 133, 1810
- Benedict, G. F., McArthur, B. E., Fredrick, L. W., et al. 2002, *AJ*, 124, 1695
- Berdnikov, L. N. & Ignatova, V. V. 2000, in *Astronomical Society of the Pacific Conference Series*, Vol. 203, IAU Colloq. 176: The Impact of Large-Scale Surveys on Pulsating Star Research, ed. L. Szabados & D. Kurtz, 244–245
- Berdnikov, L. N., Ignatova, V. V., Caldwell, J. A. R., & Koen, C. 2000, *New A*, 4, 625
- Bersier, D., Burki, G., Mayor, M., & Duquennoy, A. 1994, *A&AS*, 108, 25
- Bouchy, F., Pepe, F., & Queloz, D. 2001, *A&A*, 374, 733
- Butler, R. P. 1993, *ApJ*, 415, 323
- de Zeeuw, P. T., Hoogerwerf, R., de Bruijne, J. H. J., Brown, A. G. A., & Blaauw, A. 1999, *AJ*, 117, 354
- Derekas, A., Szabó, G. M., Berdnikov, L., et al. 2012, *MNRAS*, 425, 1312
- Eddington, A. S. 1919, *The Observatory*, 42, 338
- Ekström, S., Georgy, C., Eggenberger, P., et al. 2012, *A&A*, 537, A146
- Engle, S. G., Guinan, E. F., Harper, G. M., Neilson, H. R., & Ramage Evans, N. 2014, *ApJ*, 794, 80
- Evans, N. R. 1992, *ApJ*, 384, 220
- Evans, N. R., Bond, H. E., Schaefer, G. H., et al. 2013, *AJ*, 146, 93
- Evans, N. R., Jiang, J. H., McAlary, C. W., & Campins, H. 1993, *AJ*, 106, 726
- Evans, N. R., Szabó, R., Derekas, A., et al. 2015, *MNRAS*, 446, 4008

- Famaey, B., Jorissen, A., Luri, X., et al. 2005, *A&A*, 430, 165
- Fehrenbach, C., Duflot, M., Genty, V., & Amieux, G. 1996, *Bulletin d’Information du Centre de Donnees Stellaires*, 48, 11
- Fernie, J. D. 1966, *AJ*, 71, 119
- Fernley, J. A., Skillen, I., & Jameson, R. F. 1989, *MNRAS*, 237, 947
- Gatewood, G., de Jonge, K. J., & Stephenson, B. 1993, *PASP*, 105, 1101
- Gautschy, A. 1997, *Vistas in Astronomy*, 41, 95
- Georgy, C., Ekström, S., Granada, A., et al. 2013, *A&A*, 553, A24
- Gieren, W. P., Barnes, III, T. G., & Moffett, T. J. 1993, *ApJ*, 418, 135
- Gontcharov, G. A. 2006, *Astronomy Letters*, 32, 759
- Goodricke, J. 1786, *Royal Society of London Philosophical Transactions Series I*, 76, 48
- Gorynya, N. A., Samus, N. N., Rastorguev, A. S., & Sachkov, M. E. 1996, *Astronomy Letters*, 22, 175
- Grenier, S., Baylac, M.-O., Rolland, L., et al. 1999, *A&AS*, 137, 451
- Groenewegen, M. A. T. 2008, *A&A*, 488, 25
- Holl, B., Lindegren, L., & Hobbs, D. 2012, *A&A*, 543, A15
- Joy, A. H. 1937, *ApJ*, 86, 363
- Kharchenko, N. V., Scholz, R.-D., Piskunov, A. E., Röser, S., & Schilbach, E. 2007, *Astronomische Nachrichten*, 328, 889
- Kiss, L. L. 1998, *MNRAS*, 297, 825
- Kovacs, G., Kisvarsanyi, E. G., & Buchler, J. R. 1990, *ApJ*, 351, 606
- Kozai, Y. 1962, *AJ*, 67, 591
- Lidov, M. L. 1962, *Planet. Space Sci.*, 9, 719
- Majaess, D., Turner, D., & Gieren, W. 2012, *ApJ*, 747, 145
- Marengo, M., Evans, N. R., Barmby, P., et al. 2010, *ApJ*, 725, 2392

- Martín-Fleitas, J., Sahlmann, J., Mora, A., et al. 2014, in Society of Photo-Optical Instrumentation Engineers (SPIE) Conference Series, Vol. 9143, Society of Photo-Optical Instrumentation Engineers (SPIE) Conference Series, 0
- Mathieu, R. D. 1986, *Highlights of Astronomy*, 7, 481
- Matthews, L. D., Marengo, M., Evans, N. R., & Bono, G. 2012, *ApJ*, 744, 53
- Mérand, A., Kervella, P., Coudé du Foresto, V., et al. 2006, *A&A*, 453, 155
- Mérand, A., Kervella, P., Coudé du Foresto, V., et al. 2005, *A&A*, 438, L9
- Moore, J. H. 1913, *Lick Observatory Bulletin*, 7, 153
- Moultaka, J., Ilovaisky, S. A., Prugniel, P., & Soubiran, C. 2004, *PASP*, 116, 693
- Mourard, D., Bonneau, D., Koechlin, L., et al. 1997, *A&A*, 317, 789
- Natale, G., Marconi, M., & Bono, G. 2008, *ApJ*, 674, L93
- Neilson, H. R. & Ignace, R. 2014, *A&A*, 563, L4
- Neilson, H. R., Schneider, F. R. N., Izzard, R. G., Evans, N. R., & Langer, N. 2014, *arXiv:1412.3468*
- Pepe, F., Mayor, M., Galland, F., et al. 2002, *A&A*, 388, 632
- Perryman, M., Hartman, J., Bakos, G. Á., & Lindegren, L. 2014, *ApJ*, 797, 14
- Perryman, M. A. C. & ESA, eds. 1997, *ESA Special Publication*, Vol. 1200, *The HIPPARCOS and TYCHO catalogues. Astrometric and photometric star catalogues derived from the ESA HIPPARCOS Space Astrometry Mission*
- Raskin, G., van Winckel, H., Hensberge, H., et al. 2011, *A&A*, 526, A69
- Sahlmann, J. & Fekel, F. C. 2013, *A&A*, 556, A145
- Sahlmann, J., Lovis, C., Queloz, D., & Ségransan, D. 2011a, *A&A*, 528, L8
- Sahlmann, J., Ségransan, D., Queloz, D., et al. 2011b, *A&A*, 525, A95
- Sahlmann, J., Triaud, A. H. M. J., & Martin, D. V. 2015, *MNRAS*, 447, 287
- Sepinsky, J. F., Willems, B., & Kalogera, V. 2007a, *ApJ*, 660, 1624
- Sepinsky, J. F., Willems, B., Kalogera, V., & Rasio, F. A. 2007b, *ApJ*, 667, 1170

- Shane, W. W. 1958, ApJ, 127, 573
- Shapley, H. 1914, ApJ, 40, 448
- Storm, J., Carney, B. W., Gieren, W. P., et al. 2004, A&A, 415, 531
- Szabados, L. 2003, IBVS, 5394, 1
- Szabados, L., Anderson, R. I., Derekas, A., et al. 2013, MNRAS, 434, 870
- Turner, D. G. 1988, AJ, 96, 1565
- Udry, S., Mayor, M., Maurice, E., et al. 1999a, in Astronomical Society of the Pacific Conference Series, Vol. 185, IAU Colloq. 170: Precise Stellar Radial Velocities, ed. J. B. Hearnshaw & C. D. Scarfe, 383
- Udry, S., Mayor, M., & Queloz, D. 1999b, in Astronomical Society of the Pacific Conference Series, Vol. 185, IAU Colloq. 170: Precise Stellar Radial Velocities, ed. J. B. Hearnshaw & C. D. Scarfe, 367
- van Leeuwen, F., ed. 2007, Astrophysics and Space Science Library, Vol. 350, Hipparcos, the New Reduction of the Raw Data (Springer)
- van Leeuwen, F., Feast, M. W., Whitelock, P. A., & Laney, C. D. 2007, MNRAS, 379, 723
- Wilson, T. D., Carter, M. W., Barnes, III, T. G., van Citters, Jr., G. W., & Moffett, T. J. 1989, ApJS, 69, 951
- Zucker, S. & Mazeh, T. 2001, ApJ, 562, 549

*Facilities:* Mercator1.2m, HIPPARCOS

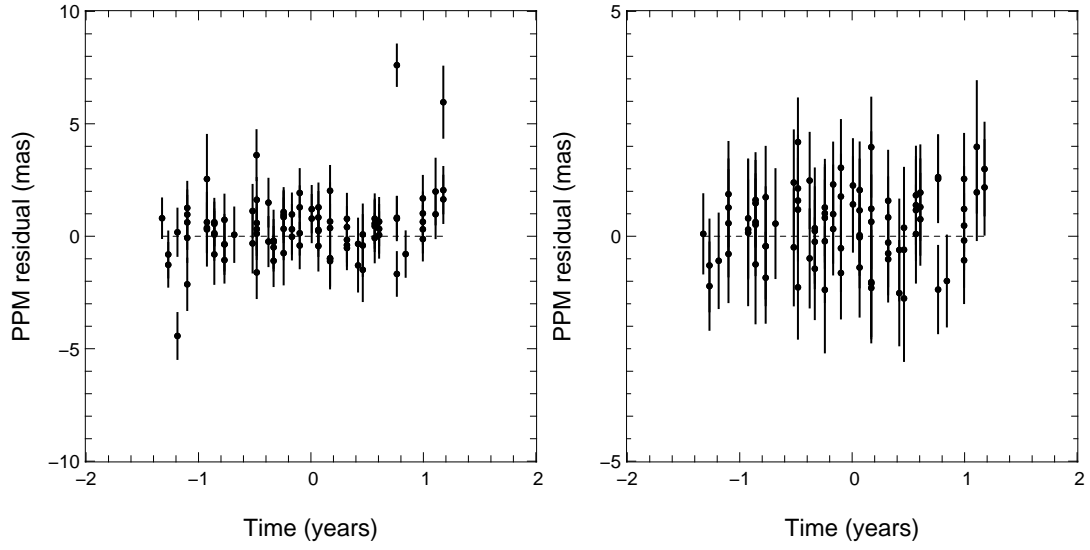


Fig. 8.— *Hipparcos* fit residuals for all 95 data points (left panel) and after removing 6 outliers (right panel). Time is relative to epoch J1 991.25 as in the original *Hipparcos* catalog (Perryman & ESA 1997).

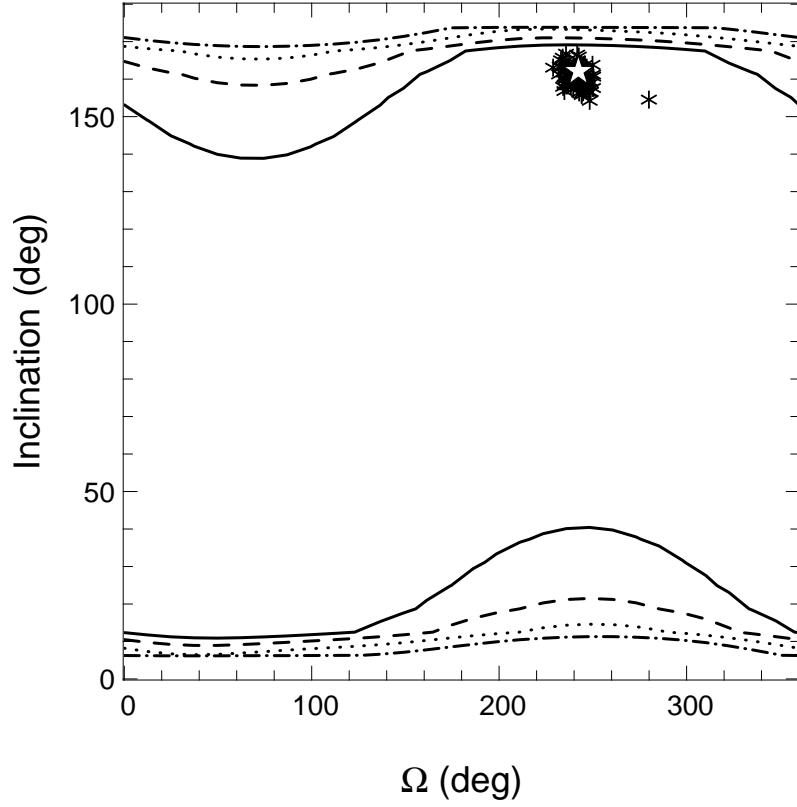


Fig. 9.— Joint confidence contours on the  $i - \Omega$ -grid. Contour lines correspond to confidence levels at  $1\sigma$  (solid),  $2\sigma$  (dashed),  $3\sigma$  (dotted), and  $4\sigma$  (dash-dotted). Crosses indicate the position of the best non-linear adjustment solution for each of the 100 Monte Carlo samples of spectroscopic parameters; the star corresponds to the adopted parameters.

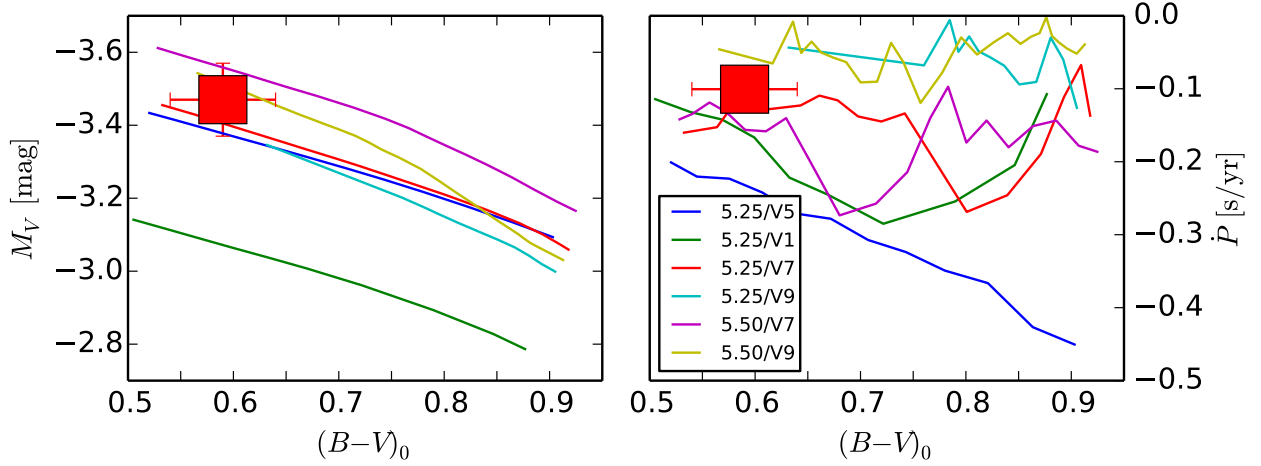


Fig. 10.—  $\delta$  Cephei’s color-magnitude and color-rate of period change diagrams that compare the measured quantities with predictions from Solar metallicity Geneva stellar evolution models (Ekström et al. 2012; Georgy et al. 2013; Anderson et al. 2014). Note that the predicted rates of period change are based on the evolution of the average density, i.e., they have not been determined from a pulsation code. We use absolute magnitude and dereddened color by Benedict et al. (2002) and the rate of period change measured by Engle et al. (2014) as the observed values. The left panel is particularly well-suited for determining progenitor mass, whereas the rate of period change is very sensitive to the main sequence rotation of  $\delta$  Cephei’s progenitor. The legend in the right panel indicates ZAMS mass in solar units followed by the model’s initial rotation rate, where V1 corresponds to  $\omega = \Omega/\Omega_{\text{crit}} = 0.1$ , V7 to  $\omega = 0.7$ , and V9 to  $\omega = 0.9$ . V5 corresponds to  $\omega = 0.568$ , i.e.,  $v/v_{\text{crit}} = 0.4$ , see Ekström et al. (2012). Comparing the observed values to model predictions (assume single star evolution),  $\delta$  Cephei is consistent with a progenitor mass of approximately  $5.25 M_{\odot}$  and slightly faster-than average surface rotation ( $\omega \sim 0.7$ ). Adopting our new parallax estimate ( $\varpi = 4.09 \pm 0.16$ ) would change  $M_V$  to  $-3.23$  mag, resulting in a lower inferred mass of  $5.0 M_{\odot}$  while yielding the same result in terms of rotation